Secreted dengue virus NS1 from infection is predominantly dimeric and in complex with high-density lipoprotein

Bing Liang Alvin Chew[1,2]†, An Qi Ngoh [3]†, Wint Wint Phoo[4]†, Kitti Wing Ki Chan[3]†, Zheng Ser[4], Nikhil K Tulsian[5,6], Shiao See Lim [3], Mei Jie Grace Weng[1,2], Satoru Watanabe[3], Milly M. Choy[3], Jenny G. Low[3,8], Eng Eong Ooi[3,9,10], Christiane Ruedl[11], Radoslaw M. Sobota[4], Subhash G. Vasudevan[3,7,12]*, Dahai Luo[1,2]*

Affiliations:

[1]Lee Kong Chian School of Medicine, Nanyang Technological University; EMB 03-07, 59 Nanyang Drive, Singapore 636921

[2]NTU Institute of Structural Biology, Nanyang Technological University; EMB 06-01, 59 Nanyang Drive, Singapore 636921, Singapore

[3]Program in Emerging Infectious Diseases, Duke-NUS Medical School; 8 College Road, Singapore 169857, Singapore

[4]Functional Proteomics Laboratory, Institute of Molecular and Cell Biology, Agency for Science, Technology and Research (A*STAR); 61 Biopolis Drive, Proteos, Singapore 138673, Singapore

[5]Department of Biological Sciences, National University of Singapore, Singapore,

[6]Singapore Centre for Life Sciences, Department of Biochemistry, National University of Singapore, Singapore, Singapore

[7]Department of Microbiology and Immunology, National University of Singapore; 5 Science Drive 2, Singapore 117545, Singapore

[8]Department of Infectious Diseases, Singapore General Hospital, Singapore, Singapore.

[9]Yong Loo Lin School of Medicine, National University of Singapore, Singapore, Singapore.

[10]Saw Swee Hock School of Public Health, National University of Singapore, Singapore, Singapore.

[11]School of Biological Sciences, Nanyang Technological University, Singapore, Singapore

[12]Institute for Glycomics (G26), Griffith University Gold Coast Campus, QLD 4222, Australia.

† These four authors contributed equally to the work.

*Corresponding author. Email: subhash.vasudevan@duke-nus.edu.sg (S.V.); luodahai@ntu.edu.sg (D.L.)

Abstract

Severe dengue infections are characterized by endothelial dysfunction shown to be associated with the secreted nonstructural protein 1 (sNS1), making it an attractive vaccine antigen and biotherapeutic target. To uncover the biologically relevant structure of sNS1, we obtained infection-derived sNS1 (isNS1) from DENV-infected Vero cells through immunoffinity purification instead of recombinant sNS1 (rsNS1) overexpressed in insect or mammalian cell lines. We found that isNS1 appeared as an approximately 250 kDa complex of NS1 and ApoA1 and further determined the cryoEM structures of isNS1 and its complex with a monoclonal antibody/Fab. Indeed, we found that the major species of isNS1 is a complex of the NS1 dimer partially embedded in a High-Density Lipoprotein (HDL) particle. Cross-linking mass spectrometry (XL-MS) studies confirmed that the isNS1 interacts with the major HDL component ApoA1 through interactions that map to the NS1 wing and hydrophobic domains. Furthermore, our studies demonstrated that the sNS1 in sera from DENV-infected mice and a human patient form a similar complex as isNS1. Our results report the molecular architecture of a biological form of sNS1 which may have implications for the molecular pathogenesis of dengue.

Summary

CryoEM structures of secreted dengue virus NS1 protein reveal dimers in complex with high-density lipoprotein.

Introduction

Dengue virus (DENV) is a member of the flavivirus genus and is the cause of significant healthcare problems and economic burden worldwide, partially due to the lack of effective therapeutics and the limited efficacy of licensed vaccines, Dengvaxia® and QDENGA®[1,2]. While the majority of DENV infections are mild or asymptomatic, severe dengue infections, marked by vascular leakage, can be life-threatening and even fatal. The severity of dengue infections has been demonstrated to be correlated to high sera levels of sNS1 in clinical studies[3,4]. The viral nonstructural protein 1 (NS1) is a highly conserved and multifunctional protein that exists as intracellular membrane-associated NS1, a presumed GPI-anchored outer

plasma membrane-associated NS1, and secreted NS1 (sNS1) during viral infection[5]. NS1 could interact with a myriad of proteins associated with its immune evasion and virotoxin roles[6]. The interactions of NS1 with viral E protein[7] and the NS4A-2K-NS4B precursor protein[8] have been shown to be important in virus production and replication respectively. Intracellular NS1 found in the ER lumen is an essential part of the membranous viral RNA replication compartment[7]. Upon release from the cells, sNS1 enters the blood circulation where *in vitro* and *in vivo* mouse evidence have demonstrated its ability to induce vascular permeability, a hallmark of severe dengue, either independently[9] or through inducing pro-inflammatory responses[10].

The high-resolution crystal structures of NS1 dimer have been reported for DENV[11], WNV[11], and ZIKV[12,13] which provide a conserved molecular view of flaviviral NS1. Mature NS1 is 352 amino acids long with an apparent molecular mass between 40 – 50 kDa depending on its glycosylation state. NS1 has a three-domain architecture, a hydrophobic β-roll (residues 1-29), an α/β wing (38-151), and a β-ladder (181-352). The connector segments between the wing and β-ladder domains, residues 30-37 and 152-180, form a 3-stranded β-sheet. The dimer has a distinct cross shape with the wings extending from the central β-ladder which has an extended β-sheet that faces the hydrophobic β-roll and a ‘‘spaghetti loop” on the opposite hydrophilic outer face that lacks structured elements[11-13]. sNS1 was reported to be a barrel-shaped hexamer with lipid cargo held together by hydrophobic interactions based on biophysical and low-resolution EM analysis[14-16]. CryoEM structures of recombinant sNS1 (rsNS1) were recently reported[17]. The rsNS1 is mainly tetrameric with only 3% of the rsNS1 population found to be in the hexameric form[17]. Other studies have implied that sNS1 interacts with high-density lipoprotein (HDL) and its major protein components, such as ApoA1 and ApoB[14,16]. Additionally, sNS1 appears to utilize the scavenger receptor B1, a known receptor for HDL, as the cognate receptor in cultured cells[17]. Since the interactions of sNS1 with the target cells implicated in pathogenesis require the hydrophobic β-roll side to be exposed[11], the mechanism by which the oligomeric sNS1 with its lipid load in the central channel dissociates and associates have been a topic of intense research interest[18-20]. However, the native structure of the extracellular NS1 during viral infection remains unclear.

To closely mimic of sNS1 circulating in dengue patients' sera, we obtained infection-derived sNS1 (isNS1) from the culture supernatant of Vero cells infected with either the DENV2 WT (isNS1wt) or T164S mutant (isNS1ts). The T164S mutation in the greasy finger loop between the wing and β-ladder interdomain of NS1 was identified from a DENV2 epidemic in Cuba in 1997, where a correlation with enhanced clinical disease severity was observed[21]. We demonstrated that this single mutation in NS1 could directly cause lethality in mice and increased sNS1 secretion[22], which served as an epidemiologically relevant tool to study the biochemical and structural characteristics of sNS1 in this study.

We determined that the isNS1 is a complex of the NS1 dimer embedded on a single HDL particle composed of ApoA1. By applying integrative structural tools, we report the cryoEM structural model of the purified isNS1:HDL complex at ~7 Å resolution with protein-protein interactions between NS1 and ApoA1 defined by crosslinking mass spectrometry (XL-MS). Furthermore, the Ab56.2 binding site model in the cryoEM model of isNS1:ApoA1 complex was elucidated using hydrogen deuterium exchange mass spectrometry (HDX-MS) as well as NS1 peptide competition ELISA. Interrogation of DENV-infected mouse sera and a human patient suggests that the sNS1:HDL complex exists *in vivo* as a similar complex to isNS1.

Results

Native isNS1 is a complex of NS1 with ApoA1

We purified sNS1 using a monoclonal antibody 56.2 from the supernatant of the infected Vero cell cultures (Fig. 1a and Supplementary Fig. 1a-b). Initial negative stain screening of the isNS1wt (Supplementary Fig. 1c) showed some 2D classes of NS1 dimers presumably docked onto a spherical density, mirroring the *in vitro* reconstitution of rsNS1 with HDL complex negative stain microscopy results by Benfrid et al. (2022)[20]. Both immunoaffinity purified isNS1wt (Fig. 1b and Supplementary Fig. 2a) and isNS1ts (Supplementary Fig. 2a and 3b) retained a molecular size of ~250 kDa as detected with Coomassie Blue (Fig. 1b and Supplementary Fig. 2a) and on a Western blot using Ab56.2 following separation on a Native-PAGE (Fig. 1b), as previously reported[22]. The isNS1wt migrated slower than the rsNS1 protein (a gift from Shu et al. 2022[23]), indicating possible conformational or oligomeric differences between the two NS1 species (Fig. 1b). On a reducing SDS-PAGE, we identified two major

bands of approximately 50 kDa and 25 kDa in isNS1wt, the former corresponding to the single monomeric NS1 band seen in rsNS1 (Fig. 1c). Preliminary mass ID identified the 25 kDa protein as bovine apolipoprotein A1 (ApoA1), a major component of HDL in bovine serum-containing culture media, which has a reported molecular weight of 28 kDa[24]. Hence, the two bands were further validated on a Western blot, which confirmed the 50 kDa band as NS1 and the 25 kDa band as ApoA1 respectively (Fig. 1c). The same observations were seen in isNS1ts (Supplementary Fig 3).

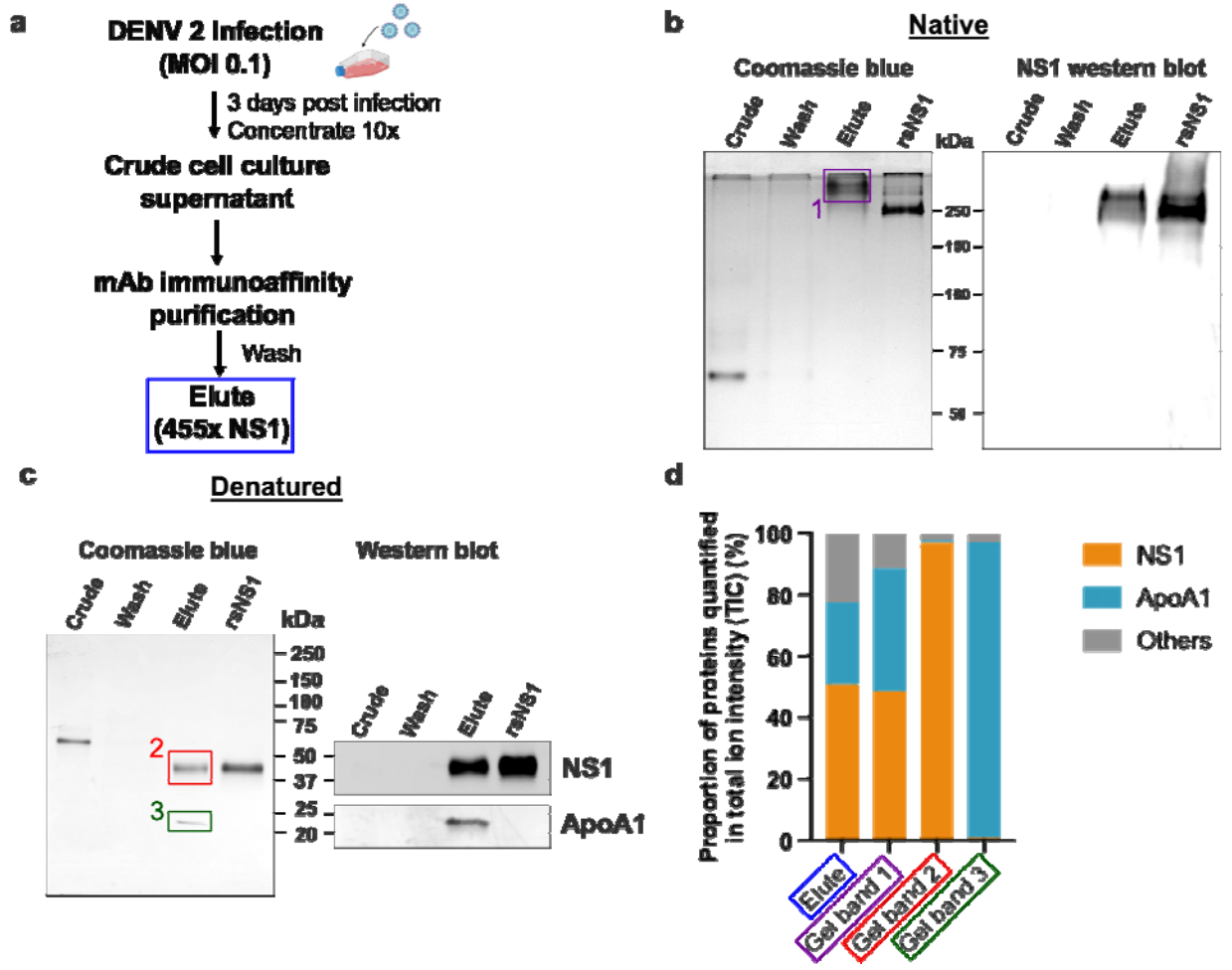

Fig. 1. Composition of the secreted NS1 from DENV-infected Vero cells. DENV 2 WT (Chan et al., 2019) cell culture supernatant was filtered, supplemented with protease inhibitor cocktail and 0.05% sodium azide, concentrated using a 100 kDa MWCO Vivaflow cassette and purified using 56.2 anti-NS1 antibody immunoaffinity chromatography as described previously (Gagnon et al., 2012). The eluted isNS1wt was dialysed against PBS, concentrated, and stored at –80°C until further use. **(a)** Schematic of isNS1 purification to illustrate the samples used for gel analyses. % NS1 is measured by the total amount of NS1 (quantified using the anti-NS1 ELISA kit (Bio-rad) as a percentage of total protein (quantified using the Bradford assay) found in each

sample. Details of the % enrichment in NS1 along the purification process is as shown in Supplementary Fig S1 B. **(b)** Coomassie blue detection of proteins from Crude, Wash and Elute immunoaffinity fractions for isNS1wt, with the recombinant sNS1 (rsNS1) obtained from Shu et al (2022) as a positive control, after separation on a 10% Native-PAGE gel (left). The Crude and Elute fractions contain 1 µg of total protein. The Wash fraction contains approximately 100 ng of total protein in maximum well volume of the gel. The same set of samples were also subjected to a western blot detection of NS1 using 56.2 anti-NS1 antibody after separation on a 10% Native-PAGE (right). The Crude and Elute fractions contain 500 ng of total protein. The Wash fraction contains approximately 100 ng of total protein in maximum well volume of the gel. **(c)** Coomassie blue detection of proteins from Crude, Wash and Elute immunoaffinity fractions for isNS1wt and rsNS1 (Shu et al., 2022), after separation on a 4-20% reducing SDS-PAGE gel. The Crude and Elute fractions contain 1 µg of total protein. The Wash fraction contains approximately 100 ng of total protein in maximum well volume of the gel. Similarly, the same set of samples were also subjected to a western blot detection of NS1 and ApoA1 using 56.2 anti-NS1 antibody or ApoA1 antibody (Biorbyt, orb10643) respectively, after separation on a 4-20% reducing SDS-PAGE (right). **(d)** In-gel protein identification of the purified isNS1wt by liquid chromatography mass spectrometry (LC-MS). Proportion of NS1, ApoA1 and other unidentified proteins quantified in total ion intensity, obtained from the following samples: Elute in solution (boxed in blue), 250 kDa gel band (boxed in purple), 50 kDa gel band (boxed in red) and 25 kDa gel band (green). The boxed gel bands are from representative gels showing the different protein species found while the actual gel bands used for protein identification by LC-MS are as shown in Supplementary Fig 2a-b.

Next, we elucidated the composition of the prominent 250 kDa band observed in the Native-PAGE by label-free quantification (LFQ) analysis of proteins using liquid chromatography–mass spectrometry (LC-MS). We obtained LC-MS data for the ~250 kDa protein excised from the Native-PAGE separation of the immunoaffinity purified isNS1wt (represented in Fig. 1b, purple box as Gel Band 1); an aliquot of the elute fraction from immunoaffinity purification (depicted in Fig. 1a blue box and referred to as “Elute”) and the 50 kDa and 25 kDa bands excised after separation of the elute fraction on a reducing SDS-PAGE (Fig. 1c, represented by red and green boxed labelled as Gel Band 2 and 3 respectively) as positive controls. The raw data for the ion intensities of the samples tested are as detailed in Supplementary File 1. We found that the combined LFQ intensity of NS1 and ApoA1 accounted for more than 77.6% and 88.6% of the total ion intensity count (TIC) detected from the elute fraction (Fig. 1a, blue box) and the 250 kDa band (Fig. 1b, the purple box labelled ‘1’) respectively, indicating that NS1 and ApoA1 were the major proteins in the elute fraction and the ~250 kDa band from immunoaffinity purified isNS1wt (Fig. 1d). Accordingly, as depicted in Fig. 1d, NS1 accounted for 96.85% of the TIC for the 50 kDa band (Fig. 1c, red box ‘2’), while the intensity of ApoA1 accounted for 96.23% of the TIC for the 25 kDa band (Fig. 1c, green box ‘3’). Similar LFQ analysis of LC-MS

data for the purified isNS1ts mutant showed that NS1 and ApoA1 were the major components (Supplementary Fig. 2) of the respective Elute and ~250 kDa gel band on Native-PAGE (Supplementary Fig. 2a; 3a, purple box). The corresponding 50 kDa and 25 kDa gel bands on the reducing SDS-PAGE (Supplementary Fig. 2b, 3b) identified as NS1 and ApoA1 by immunoblotting with the respective antibodies (Supplementary Fig. 3b), were further confirmed by LC-MS as NS1 and ApoA1 (Supplementary Fig. 2c, 3c, Supplementary file 1). Taken together, the results from the Native PAGE and LFQ by LC-MS strongly indicated that the isNS1 purified from the supernatant of infected cells *in vitro* is an approximately 250 kDa complex of NS1 and ApoA1.

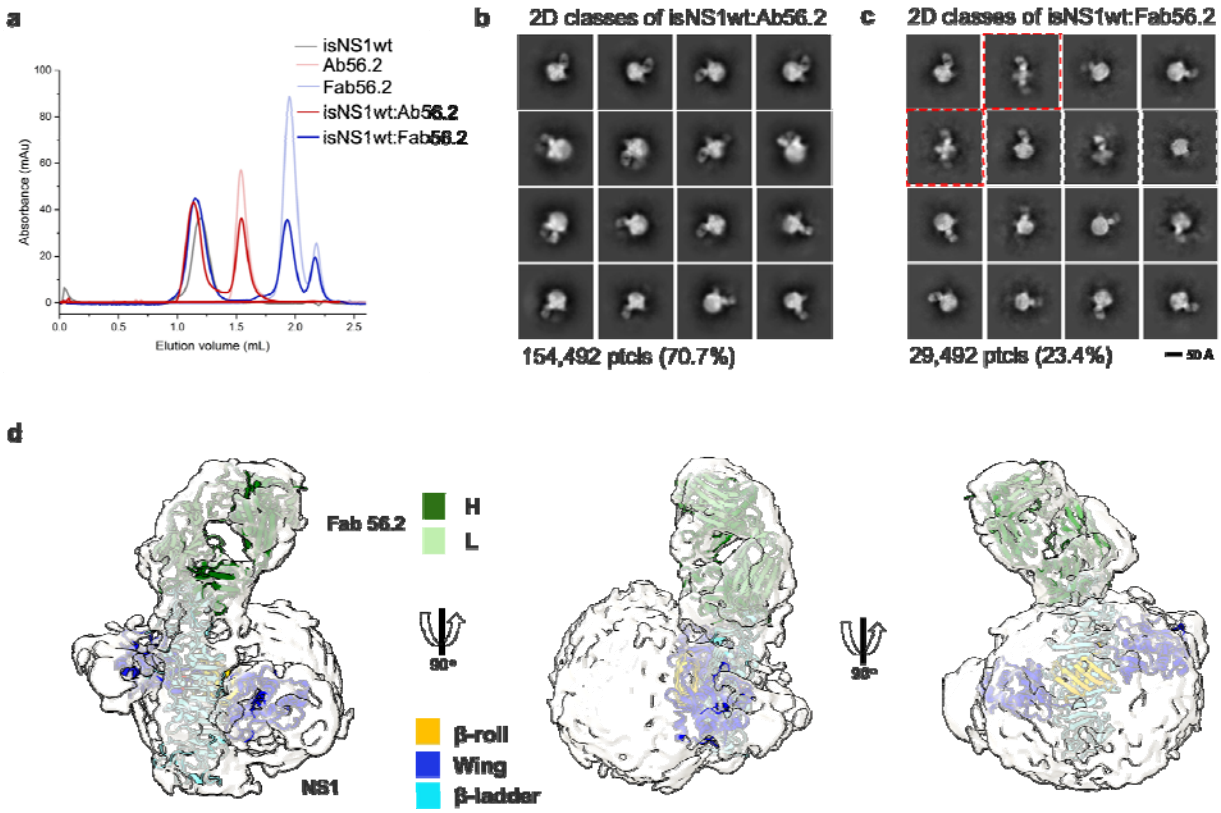

Fig. 2. CryoEM analysis of secreted NS1 in complex with antibody Ab56.2. (a) Size exclusion chromatography was run on a Superdex 200 increase 3.2/300 GL column connected to the ÄKTA purifier with a flow rate of 0.075 mL/min in PBS (pH 7.4) for purified isNS1wt (gray), Ab56.2 (faded red), Fab56.2 (faded blue), isNS1wt:Ab56.2 (red) and isNS1wt:Fab56.2 (blue). A slight leftward shift in elution volume was observed for isNS1wt upon complexing with Ab56.2 and Fab56.2. 2D class averages of **(b)** isNS1wt:Ab56.2 and **(c)** isNS1wt:Fab56.2 showing representative sub-class of the Fab56.2:isNS1:HDL particles with black scale bar, 50 Å. The corresponding number of particles and percentages are listed below the respective boxes. Red dashed line boxes highlight two rare views consisting of 1033 particles (3.5%) only seen in

isNS1wt:Fab56.2 sample. **(d)** Model of isNS1wt:Fab56.2 predicted structures rigid body fitted in the CryoEM map of Fab56.2:isNS1:HDL (grey, contoured at 0.14) with correlation value of 0.75 to the fitted regions (map simulated from atoms at 5 Å). isNS1wt is coloured by its three domains, namely the β-roll (orange), wing (blue), and β-ladder (cyan). Fab56.2 is coloured by its heavy chain (dark green) and light chain (light green).

CryoEM structure of isNS1

To gain insights into the molecular organization of this native isNS1, we determined the cryoEM structure of isNS1 (Supplementary Table 1 and Supplementary Fig. 4-7). The 2D classes of isNS1ts are observed to be heterogenous spheres with some internal features, some of which resembling the cross-shaped NS1 protruding from the sphere (Supplementary Fig. 4b). However, the 3D reconstruction of isNS1ts alone was observed to have no discernible features beyond a spherical-like density with varying dimensions averaging around 106 Å by 77 Å (Supplementary Fig. 4). To obtain higher resolution structural information on the complex, we collected data for the ternary complexes of the isNS1wt:Ab56.2, isNS1wt:Fab56.2 and the isNS1wt:Fab56.2 (Fig. 2a and Supplementary Fig. 5-6). The use of antibodies as fiduciary markers is a well-proven approach for solving the structures of small proteins[25,26]. Overall, both samples resulted in similarly distinguishable 2D class averages (Fig 2b-c) which show asymmetrical binding of one unit of Fab56.2 to the dimeric cross-shaped sNS1 associated with a lower-density sphere, presumably HDL.

In the isNS1wt:Fab56.2 ternary complex dataset, we further observed two apparent but rare sub-classes of free sNS1wt dimer bound to two units of Fab56.2 representing 3.5% of the total population of picked particles (Fig. 2c, red dashed boxes). While the cryoEM map reconstructions remain limited at low resolutions (Supplementary Fig. 5-6), they could be fitted with the NS1 dimer and Fab56.2 models (Fig. 2d) predicted separately using AlphaFold[27,28], with a correlation value of 0.75 to the fitted regions using a simulated 5 Å map from the NS1 dimer and Fab models. The AlphaFold predicted model of the NS1 dimer was used despite the availability of the crystallographic dimer model (PBS ID: 6WER) because the latter had a few unmodelled residues (aa 118-128)[7,11]. The predicted model upon superimposition on the crystallographic model, nonetheless, has a RMSD of 0.67 Å indicating that these two models were highly similar[29]. The map-model fitting showed that the epitope sites were at the tip of the C-terminal β-ladder region. The approximate dimensions of the spherical HDL could also be

measured at 82 Å by 65 Å (Supplementary Fig 5-6) which aligned with existing reports of spherical HDL being measured at 70-120 Å in diameter with predominantly homodimeric ApoA1 arranged as an anti-parallel double-belt stabilized by intermolecular salt bridges[30,31]. We predicted a model of an antiparallel dimer of ApoA1 using AlphaFold2[27,28] without the first 58 residues of ApoA1 as the N-terminal domain is highly flexible[30]. The model has a cross-sectional distance of approximately 78 Å and fits into the spherical density in the cryoEM map. The NS1 dimer appears semi-embedded on the HDL particle through its hydrophobic surface, with a conformation that exposed only one end of the β-ladder domain to which Ab56.2 and Fab56.2 bind. Overall, the cryoEM model indicated that the purified ~250 kDa isNS1 is a complex of a NS1 dimer and HDL, consistent with the gel and LFQ analysis of LC-MS data presented above.

Similarly, we determined the structures of the ternary complex of isNS1ts mutant with Fab56.2 (Fig. 3a). Interestingly, 2D class averages of isNS1ts:Fab56.2 dataset showed a significant sub-population of a free NS1ts dimer bound to two units of Fab56.2 (53.7%), in addition to the HDL spheres (23.6%) and isNS1ts dimer:HDL:Fab56.2 (22.7%) classes (Fig. 3b and Supplementary Fig. 7). The predicted structure of the isNS1ts dimer bound to Fab56.2 could be fitted with an overall correlation value of 0.5 using map simulated from atoms at 5 Å (Fig. 3c). Achieving atomic resolution to map the Fab binding interface with the NS1 β-ladder domain remains a challenge due to the preferred orientation (Supplementary Fig. 7). A comparison of the cryoEM density maps of free isNS1ts dimer:Fab56.2 (Fig. 3D, grey) and isNS1ts dimer:HDL:Fab56.2 ternary complex (Fig. 3d, yellow) fitted with a correlation value of 0.71 based on the NS1 map region, revealed a pose difference of the Fab56.2 between the free isNS1ts dimer and the HDL-bound isNS1ts dimer (Fig. 3d, inset). Further comparison of the density maps of the isNS1 dimer:HDL population in the Fab56.2 ternary complexes of isNS1wt (Fig. 3e, purple) and isNS1ts (Fig. 3e, yellow) revealed conformational similarities of the isNS1 dimer:HDL complex.

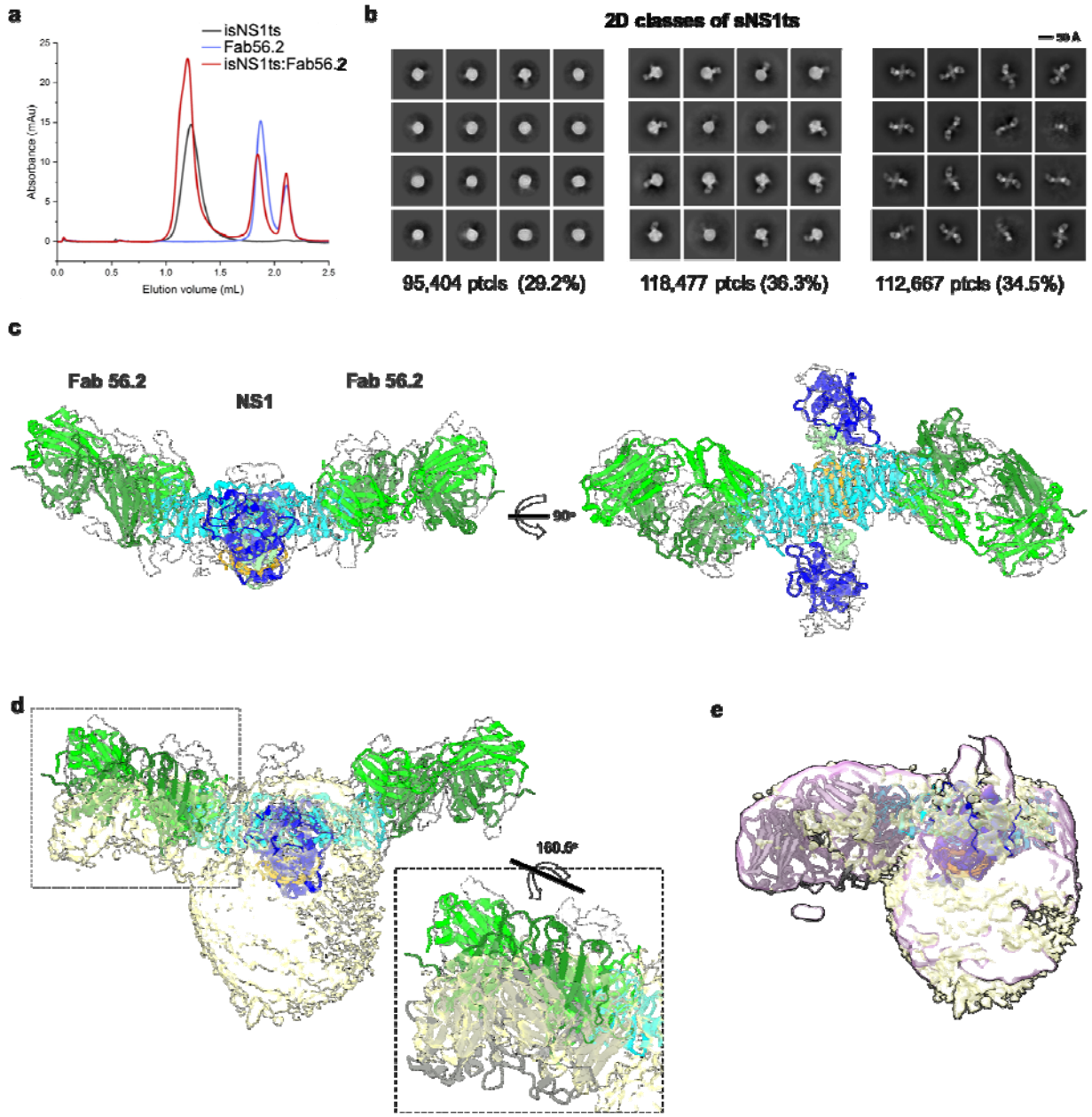

Fig. 3. Secreted NS1 forms free dimers in complex with antibody Ab56.2. (a) Size exclusion chromatography was run on a Superdex 200 increase 3.2/300 GL column connected to the AKTA purifier with a flow rate of 0.075mL/min in PBS (pH 7.4) for purified isNS1ts (gray), Fab56.2 (faded blue) and isNS1ts:Fab56.2 (red). A similar leftward shift in elution volume was also observed for isNS1ts upon complexing with Fab56.2. **(b)** 2D class averages of isNS1ts:Fab56.2 dataset with 326,548 particles picked and separated into 3 distinct populations, HDL spheres, Fab56.2:isNS1:HDL, and free isNS1:Fab56.2. Black scale bar, 50 Å, as indicated. The corresponding number of particles and percentages are listed below the respective boxes. **(c)** Model of isNS1ts dimer and Fab56.2 predicted structures rigid body fitted in the isNS1ts:Fab56.2 density map (grey, contoured at 0.14) with correlation value of 0.53 (overall, map simulated from atoms at 5 □). isNS1ts is coloured by its three domains, namely the β-roll

(orange), wing (blue), and β-ladder (cyan). Fab56.2 is coloured by its heavy chain (dark green) and light chain (light green). **(d)** Density map fitting between isNS1ts:Fab56.2 (grey, contoured at 0.14) to Fab56.2:NS1ts:HDL (yellow, contoured at 0.1) with correlation value of 0.53 (overall) and 0.7137 (on D2NS1 map region only). Inset shows the difference in the pose of Fab from the free NS1 form to the HDL-bound form. (e) Density map fitting between Fab56.2:isNS1wt:HDL (purple, contoured at 0.05) to Fab56.2:NS1ts:HDL (yellow) with correlation value of 0.72 (overall).

XL-MS maps the inter- and intra-molecular architecture of the isNS1

Next to refine our understanding of the NS1 dimer:HDL complex of the isNS1 indicated by the LFQ of LC-MS (Fig. 1d and Supplementary Fig. 3d) and cryoEM results (Fig 2d and 3d), we probed the interactions between NS1 and ApoA1 - the major protein moiety of HDL - using crosslinking mass spectrometry (XL-MS)[32] on the immunoaffinity purification eluate fraction (Fig. 4a, Supplementary Fig. 8a-b). We identified 28 NS1:NS1 and 29 ApoA1:ApoA1 intramolecular crosslinks, as well as 25 NS1:ApoA1 intermolecular crosslinks for isNS1wt (Fig. 4b; Supplementary File 2a-b). As depicted in Fig. 4b-c, the NS1 residues that are involved in both intra- and inter-molecular crosslinks were located mainly on the β-roll and wing domains, with ~34% of the NS1:ApoA1 crosslinks being located on the β-roll domain. The NS1:NS1 intramolecular crosslink pairs were further validated on the predicted NS1 dimer model by implementing a 30 Å cut-off distance for the Cα atoms of crosslinked residues, a criterion that was met by 85% of the NS1:NS1 intramolecular crosslinks (24 out of 28; Fig. 4d). The NS1:ApoA1 intermolecular crosslinks for the immunoaffinity purified isNS1wt were found to be located between the β-roll and wing domains of NS1 and the helices 3, 4, 8 and 10 of ApoA1 (Fig. 4b, d). Applying the same cut-off value of <30 Å distance between the Cα atoms of the NS1:ApoA1intermolecular crosslinked residues and validating it on the cryoEM model of isNS1wt in this study (Fig. 4d-e) satisfied 76% of the crosslinks (19 out of 25 intermolecular crosslinks between NS1 dimer and ApoA1). In the case of ApoA1:ApoA1 intramolecular crosslinks, the <30 Å distance between their Cα atoms cut-off satisfied 62% of the crosslinks (18 out of 29 ApoA1:ApoA1 intramolecular crosslinks). The higher number of violated crosslinks in ApoA1:ApoA1 compared to those in NS1:NS1 could be due to the flexible and dynamic nature of ApoA1 dimers which may prevent it from assuming a fixed relative position among the ApoA1 dimer population in the HDL. Overall, the XL-MS data and structural validation agreed with the cryo-EM model of isNS1 being a complex of the NS1 dimer embedded on a HDL particle composed of an ApoA1 dimer (Fig 4d-e).

Additionally, the XL-MS mapping of isNS1ts mutant (Supplementary Fig. 8c-d) followed by rigid-body fitting into the corresponding cryoEM map (Supplementary Fig. 8e) revealed a similar crosslink pattern to isNS1wt, except that there were fewer crosslink sites (Supplementary Fig. 8f, Supplementary File. 2a). This indicated that isNS1ts dimer may have a weaker affinity to HDL in comparison to the isNS1wt dimer. This finding is consistent with the cryoEM data for isNS1ts where we found that free isNS1ts dimers bound to Fab56.2 formed a significant sub-population (34.5%) of the total picked particles (Fig. 3b, Supplementary Fig. 7b).

Given the reported structures of hexameric and tetrameric rsNS1 from mammalian expression systems, insect cells[11,15,16,29] and Expi293 HEK cells[33], we further examined whether rsNS1 oligomerizes in the presence of exogenously added human HDL, using XL-MS. The crosslinked rsNS1 alone appeared as higher oligomer bands of dimers, tetramers, and hexamers on the SDS-PAGE analysis (Fig. 4f, lane 3) which differed from the crosslinked isNS1 (Fig 4f, lane 3). Interestingly, the addition of human HDL and crosslinker resulted in a smearing band ranging from 30-150 kDa with the loss of the well-defined monomeric rsNS1 band (Fig 4f, lane 4). In the crosslinked rsNS1 in the absence of HDL, we identified 17 NS1:NS1 intramolecular crosslinks at the β-roll and wing domains (Fig. 4f-g, Supplementary File 3a-b). In the presence of human HDL, we identified 30 ApoA1:ApoA1, 4 NS1:NS1, and 6 NS1:ApoA1 crosslinks (Supplementary File 3a-b). Most crosslinks identified are ApoA1:ApoA1 intramolecular crosslinks in the rsNS1:ApoA1 samples (Fig. 4g). Only 1 out of 6 rsNS1:ApoA1 intermolecular crosslinks was within the 30 Å cutoff distance when mapped to the NS1:ApoA1 cryoEM model (Fig. 4e). This was in stark contrast with the isNS1 samples where the number of crosslinks between ApoA1:ApoA1, sNS1:sNS1, and sNS1:ApoA1 was similar (Fig 4b). Overall, this suggests that rsNS1 may form oligomers of dimers but not a complex with HDL under the tested conditions.

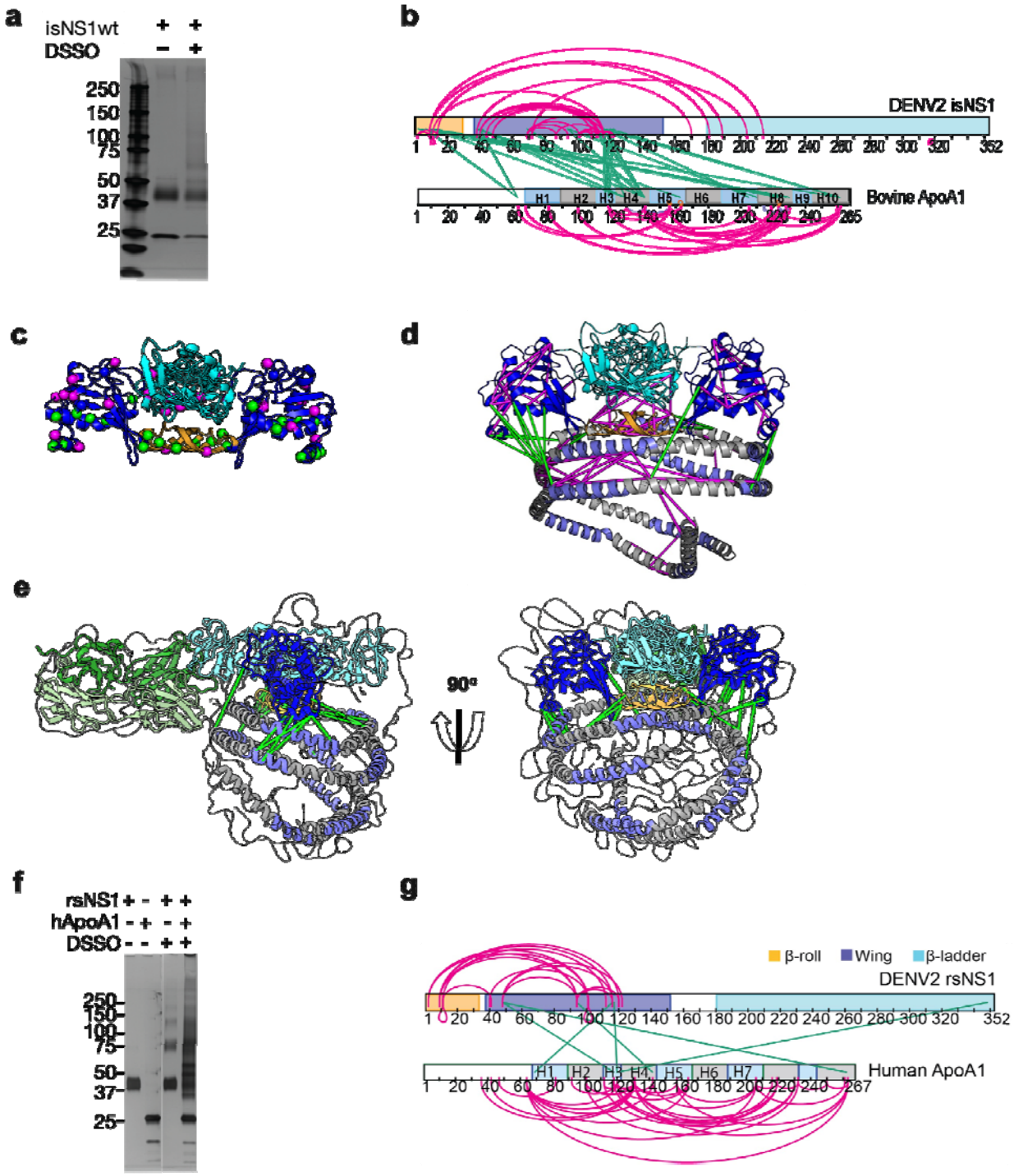

Fig. 4. Interaction sites of NS1:ApoA1 complex identification by crosslinking mass spectrometry. (a) SDS-PAGE analysis of isNS1wt with or without the addition of DSSO crosslinker. **(b)** The identified crosslinks are visualised on the NS1 and bovine ApoA1 constructs. The intramolecular (NS1:NS1 and ApoA1:ApoA1) crosslinks are in magenta. The intermolecular NS1:ApoA1 crosslinks are in green. **(c)** The isNS1 residues that are involved in NS1:NS1 interactions are visualised on the NS1 dimer model. The NS1 cartoon model is coloured by its three domains, namely the β-roll (orange), wing (blue), and β-ladder (cyan) with

the intramolecular (magenta) and intermolecular (green) crosslinking sites depicted as spheres. **(d)** The overall model interpretation of NS1:ApoA1 complex within the crosslinker theoretical distance cut-off at =< 30 Å as depicted. ApoA1 dimer cartoon model with its conserved helices as labelled coloured in intervals of grey and light purple. **(e)** The NS1:ApoA1 dimer model with validated crosslinks were fitted into the cryoEM envelope. **(f)** SDS-PAGE analysis of crosslinked rsNS1 alone or with human HDL **(Lanes 3-5)**. Non-crosslinked rsNS1 and Human HDL are the control **(Lanes 1-2)**. The crosslinked rsNS1 can be seen in higher oligomers **(Lane 3)**. **(g)** Identified crosslinks are mapped on the NS1 and ApoA1 constructs, coloured as per panel B.

Ab56.2 binds at the C-terminal β-ladder region of NS1

The cryoEM map for isNS1wt:Fab56.2 reliably placed the epitope site of Ab/Fab56.2 at the C-terminal b-ladder region, although the precise identification of the epitope site was hindered by the limited resolution of the cryoEM maps (Fig. 2-3, Supplementary Fig. 4-7). Attempts to improve the resolution were challenging so we resorted to using a truncated form of recombinant secreted NS1 consisting of only the C-terminal region (rsNS1c; residues 172-352) to determine Ab56.2 epitope. The rsNS1c fragment of residues 172-352 was previously used for structural studies of dengue[34,35] and other flaviviruses, West Nile virus[34], Zika virus[35 36], and Japanese encephalitis virus[37]. The epitope region of Ab56.2 was first confirmed by overlapping 15-mer NS1 peptide competition ELISA for Ab56.2 binding (Supplementary Fig. 9a, Supplementary Table 2). The greatest competition was observed at the NS1 peptide spanning residues 316-330 out of 301-340 which showed a decrease in OD450 absorbance (Supplementary Fig. 9b). We further applied the hydrogen-deuterium exchange mass spectrometry (HDX-MS) to monitor the conformational dynamics between Fab56.2 and NS1c to obtain higher peptide-level resolution for the binding interface. Comparative HDX results revealed global scale protection against deuterium exchange of NS1c in the presence of Fab56.2 (Fig. 5a, Supplementary Fig. 10a), indicative of reduced conformational dynamics. Large-scale differences in deuterium exchange were primarily observed across peptides spanning the dimer interface (residues 174-186) and at the tip of the C-terminal β-ladder (residues 286-347) of NS1c (Fig. 5b). Multiple overlapping peptides, spanning residues 286-347 (Fig. 5b), showed protection against deuterium exchange even at the longer labeling times (100 min) in NS1c:Fab56.2 complex (Supplementary Fig. 10a, Supplementary File 4). These results suggest that Fab56.2 bound stably with NS1c. Coupled with the observation that the most significant change in the differential plot was at residues 300-310

(Fig. 5a), these results collectively indicate that NS1c binds stably to Fab56.2 at the primary epitope site of residues 300-310.

Comparative HDX results of NS1c-bound and free Fab56.2 revealed protection against deuterium exchange of all three complementarity-determining regions (CDR) of the heavy chain (Fig. 5c, Supplementary Fig. 10b) and CDRL2 of the light chain (Fig. 5d, Supplementary Fig. 10c). Upon binding to NS1c, peptides spanning CDRH3 (residues 89-116) showed the largest magnitude decrease in deuterium exchange at all labeling time points, while CDRH2 showed minor significant differences. In addition, only the CDRL2 loop (residues 49-56) of the light chain of Fab56.2 showed significantly decreased deuterium exchange. Mapping of the deuterium exchange profiles of heavy and light chains onto a model of Fab56.2 (Fig. 5e) revealed that CDRH1-3 and CDRL2 loops were spatially co-localized to form the paratope site to bind NS1c, with the heavy chain being the primary anchor. Collectively, these results indicated that residues 300-310 of NS1 act as the primary epitope site to bind Fab56.2 and Fab56.2 binds stably with NS1c.

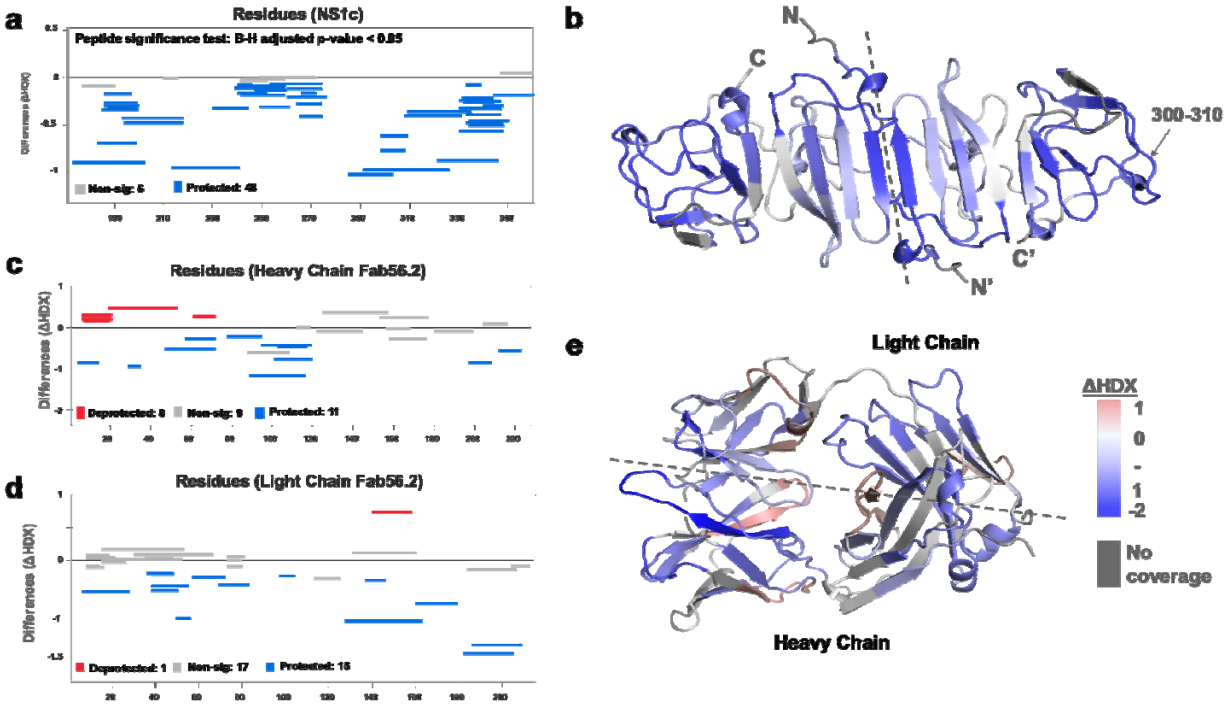

Fig. 5. Interaction interface of rsNS1c-Fab562 complex characterized by HDX-MS. (a) Woods differential plot showing the differences in deuterium exchange (y-axis) between Fab562-bound and free NS1c protein across various residues (x-axis) at 10 min labeling timepoint. Negative differences indicate protection against deuterium exchange across NS1c

peptides in the presence of Fab562, as compared to free NS1c. A p-value <0.05 is considered as significance threshold, which identified 6 non-significant peptides (grey lines) and 48 protected peptides (blue lines). **(b)** Cartoon representation of NS1c dimer model showing differences in deuterium exchange at 10 min labeling as indicated in key. Dashed line distinguishes the two monomers in the dimer. Peptide spanning residues 300-310 showing the highest protection are indicated. **(c, d)** Woods differential plot comparing the differences in deuterium exchange of Fab562 in the presence and absence of NS1c for various peptides of **(c)** heavy chain, and **(d)** light chain. A p-value <0.05 is considered as significance threshold, which identified deprotected (red lines), non-significant, and protected peptides as indicated. **(e)** Cartoon representation of Fab562 model showing deuterium exchange differences at 10 min mapped for Fab562-NS1c complex, as per key. Plots were generated using Deuteros 2.0, while cartoon structures were generated using PyMoL.

Circulating NS1 is in the form of NS1:HDL complex

Lastly, we sought to provide *in vivo* evidence of NS1 and ApoA1 interaction using sera samples from DENV-infected mice and a human patient. Since we previously showed that DENV2 T164S mutant virus led to more severe disease in the AG129 mouse model[22], we used the same infection model to obtain pooled mice serum for immunoaffinity purification of sNS1ts as described in Supplementary Fig. 1. The mouse sera immunoaffinity purified sNS1ts was detected at ~250 kDa by both anti-ApoA1 and anti-NS1 antibodies in a Western blot analysis following separation on a Native PAGE (Fig. 6a), supporting our mass spectrometry finding that ApoA1 is part of the ~250 kDa isNS1 protein complex purified from infected Vero cells (Fig. 1d). We next examined if the isNS1:HDL complex can be detected in dengue patients using serum samples obtained from the CELADEN clinical trial[38]. A primary infection sample with high levels of sNS1 (>15 µg/ml) detected by commercial Platelia™ NS1 ELISA was selected for this purpose to avoid the confounding factor of the presence of anti-NS1 Abs in the secondary infected patients and to pull-down sufficient sNS1 from the patient serum. The patient serum was first subjected to a pre-clearing step using Protein AG resin to reduce the abundance of human IgGs that may interfere with the downstream analysis. We then subjected the pre-cleared patient serum to immunoprecipitation using commercial polyclonal anti-ApoA1 antibodies to pull down and detect ApoA1 and possibly sNS1. Increasing the anti-ApoA1 antibody from 10 to 50 µg coupled onto Protein AG resin for pull-down resulted in a corresponding increase in the sNS1 amount detected by ELISA (Fig. 6b), suggesting a specific association between sNS1 and ApoA1. Collectively, despite the limited amount of sNS1 in sera samples from DENV-infected mice or humans, our data points to the association of ApoA1 with sNS1 *in vivo*.

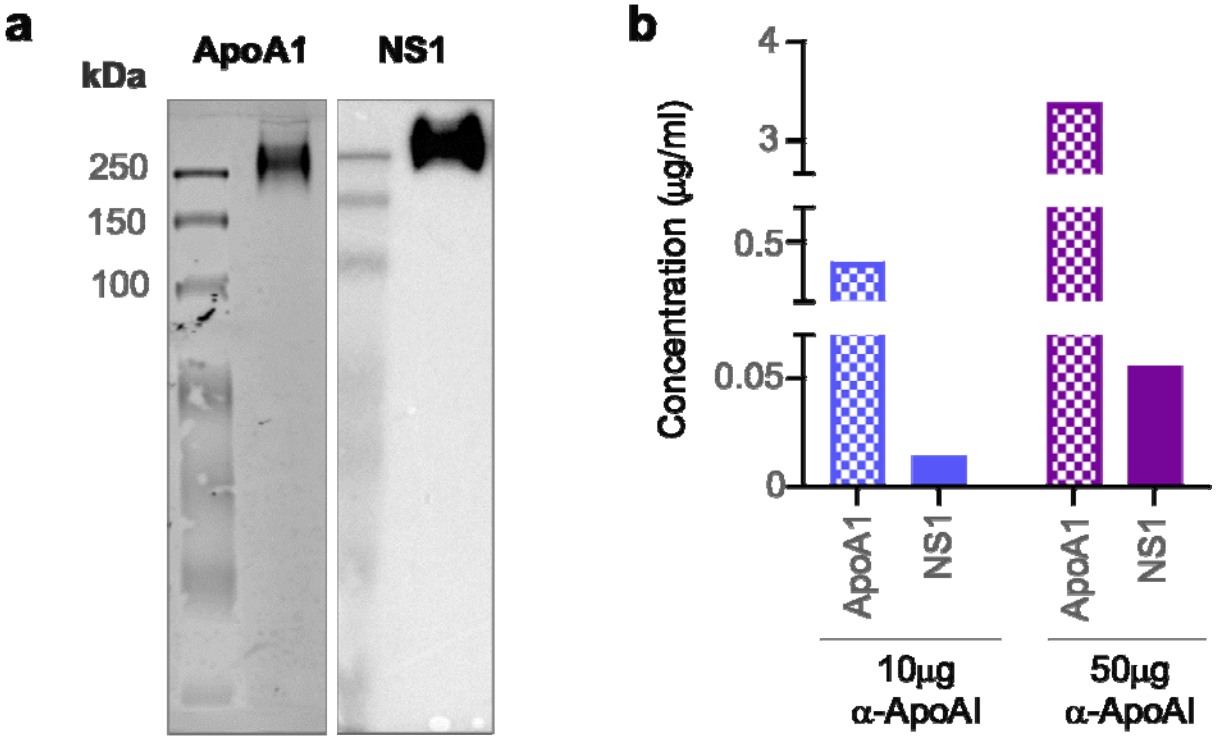

Fig. 6. sNS1 associates with ApoA1 in DENV infected mouse and human serum. (a) AG129 mice (n = 10) were infected with DENV2 NS1 T164S mutant virus and the pooled infected sera collected on day 4 post-infection was subjected to NS1 immunoaffinity purification using anti-NS1 56.2 coupled resin as in Supplementary Fig. 1. 2 mg of the purified eluate was then subjected to Western blot analysis after separation and transfer from Native PAGE for detection of ApoA1 and NS1. ApoA1 was detected using the mouse monoclonal anti-ApoA1 clone 513 (Invitrogen, MIA1404) **(left panel)** and the oligomeric NS1 was detected using anti-NS1 56.2 IgG clone **(right panel)**. **(b)** Protein AG resin (Pierce) pre-cleared DENV1 infected patient serum (n = 1) from the CELADEN trial (Low et al., 2014) was immunoprecipitated with 10 or 50 mg of rabbit polyclonal anti-ApoA1 antibody (Biorbyt, orb10643) to detect association between ApoA1 and NS1 by ELISA. The amount of ApoA1 and NS1 in the immunoprecipitated sample was determined by human ApoA1 (Abcam, ab189576) and Platelia™ NS1 Ag (Bio-Rad) ELISAs.

Discussion

In this study, by integrating biochemical and biophysical approaches including immunoaffinity purification, cryoEM, XL-MS and HDX-MS, we have successfully purified and characterised a native population of isNS1. We determined the cryo-EM structure of a natively secreted NS1 from DENV2-infected cells as a ternary complex of NS1 dimer embedded on a single HDL particle. The structure is validated by in-solution cross-linking mass spectrometry (XL-MS) analysis of the cryoEM samples. The NS1:ApoA1 complex is mediated through defined

interactions between the β-roll and wing domains of NS1 and helices 3, 5, 8, and 10 of (bovine) ApoA1 – the main protein moiety of HDL. Additionally, we were able to preliminarily observe NS1:HDL complexes in purified sNS1 from the sera of DENV2-infected mice and further detect and quantify NS1 that co-immunoprecipitated with ApoA1 in the serum of a DENV1-infected patient, further supporting the *in vivo* and clinical relevance of the NS1:HDL complexes. We also captured a population of free sNS1 dimers that are bound to two copies of Fab56.2 from the same sample. These sNS1 dimers may be separated from HDL complex or the oligomeric form upon Fab56.2 binding. There may be a dynamic equilibrium between the HDL-bound NS1 and oligomeric NS1, regulated by an interplay between NS1 secretion and circulating HDL.

Secreted NS1 from DENV1-infected cells was shown to be a detergent-labile complex of ~300 kDa that contains lipid species similar to that of HDL[14]. Benfrid et al. (2022) recently reported that dimers of rsNS1 bind to HDL when healthy plasma was spiked with purified rsNS1 and subsequently immunoaffinity purified[20]. Indeed, for the ~250 kDa PAGE band that was thought to be hexameric[14-16], it could be a complex of dimeric NS1 (~100 kDa) with HDL (~164 kDa reported by Benfrid et al., 2022[20]) composed of ApoA1 homodimer (~50 kDa) arranged as an antiparallel dimer along with the lipids. Similar to our isNS1 findings, NS1 dimers from the rsNS1 were found to be anchored on the surface of the spheroid human HDL particles, albeit in varying ratios from one to three dimers docked on a single HDL particle [15]. These differences in ratios could be attributed to variations in the concentration of sNS1 used for spiking and immunoaffinity purification. The concentration of the rsNS1 (400 μg/mL) used for spiking in the mentioned study was more than 10-fold higher than that in the concentrated crude supernatant we used for immunoaffinity purification (~30 μg/mL). Given that circulating spheroid HDL can consist of two or more copies of ApoA1 in a double-belt model or multifoil model[39] respectively within the same HDL population, it is theoretically possible that under high concentrations of rsNS1, the NS1 dimers could associate with multiple ApoA1 molecules on the HDL particle. Nonetheless, the structure of a NS1 dimer docked onto a single HDL particle is likely to be more physiologically relevant, considering that the concentration used in our study is closer to the maximum clinically reported concentration of sNS1 in the sera of DENV patients (50 μg/mL)[3,40,41]. Furthermore, the observation that NS1 interacts with HDL regardless of the source of mammalian ApoA1 is unsurprising, given the high sequence similarity of bovine and mouse

HDL to human HDL of approximately 79% and 65% respectively (Supplementary Fig. 11) and that the structure of ApoA1 is highly conserved due to the functional significance of the amphipathic α-helices in HDL assembly and lipid interactions.

While we observed a significant number of NS1:ApoA1 crosslinks (29 crosslinks, Fig 4b) via XL-MS in isNS1wt, only 6 NS1:ApoA1 crosslinks (Fig 4g) were detected between rsNS1 and HDL, suggesting weaker interaction between the two species compared to that in the isNS1 complex. However, the reconstitution experiment in the aforementioned study demonstrated that rsNS1 could disassemble into its dimeric building blocks in the presence of human serum, allowing for anchorage onto HDL particles[20]. These findings collectively suggest that once the higher-order oligomers of NS1 dimers are formed, they become highly stable and may require assistance from other serum proteins to dissociate and bind to HDL. HDL is known to recruit and interact with at least 96 different serum proteins for its functions[42,43]. Alternatively, it could be due to the difference between insect cell (*Drosophila* S2)-expressing rsNS1 used in the reconstitution experiment[20] and the commercial HEK293-expressing rsNS1[10,44] used in our study for crosslinking with purified human HDL. Hexamers were reported in insect cell-expressing rsNS1[15,16] while tetramers were the predominant form from Expi293F-expressing rsNS1[33]. Hence, such structural differences may affect the binding pattern between the two different sources of rsNS1. Overall, the intermolecular interaction residues identified using in-solution XL-MS (Fig. 4b) do support the fitted 3D model of isNS1 as a complex of NS1:HDL (Fig. 4d-e; Supplementary Fig. 8e).

High molecular weight recombinant NS1 was also interpreted to be a hexameric NS1 oligomer based on results obtained from SEC, SAXS, chemical crosslinking, negative staining EM methods, and crystallographic packing analysis[11,14,15] depicted in Supplementary Fig. 12a. Shu et al. (2022) recently reported the first high-resolution cryoEM structure of rsNS1 that is predominantly tetrameric with two NS1 dimers interacting with each other via the hydrophobic interactions[33], with only ~3.1% out of all rsNS1 particles in the hexameric form[33] (Supplementary Fig. 12b). However, these hexamer models highly disagree with our XL-MS data (Fig. 4b, Supplementary Fig. 8c) since the β-roll domain in these models is presumably forming the lipid core with little space (~17 – 20 Å) for interaction with another protein. Hence,

it is improbable to accommodate the ApoA1 at the core of the hexamer which we illustrated in Supplementary Figure 12a-c using a sphere with a radius of 30 Å to represent the maximum range between the Cα atoms that can be cross-linked to the β-roll (residue Ser2). These multimeric NS1 species may still co-exist with NS1:HDL during viral infection given that rsNS1 form oligomers such as tetramers and hexamers in the absence of ApoA1 and its associated lipid content from HDL. Furthermore, the presence of a significant population of free isNS1ts dimers in complex with Fab56.2 and fewer crosslinks identified between isNS1ts and ApoA1 point towards the possibility that isNS1ts is more dynamic in its association with host proteins than isNS1wt. The dynamic picture of the different forms of sNS1 that is further enriched in the presence of anti-NS1 antibodies has been recently reviewed [5,45,46].

Finally, the detection and quantification of sNS1 from an ApoA1 pull-down using commercial antibodies in DENV1-infected patient serum[38] provided preliminary evidence that HDL-bound sNS1 complexes are clinically relevant. This is irrespective of the source of mammalian ApoA1 which are highly conserved in sequence and length, for which human and bovine ApoA1 shares ~78% sequence identity (Supplementary Fig. 11). Although the sample size of mice and dengue patient is small and the NS1 antibodies could bind to serum proteins non-specifically, our observation of sNS1 association with ApoA1 from *in vivo* natural infection is supported by Benfrid et al. (2022) study which detected sNS1 in complex with HDL in the sera of hospitalized DENV patients[20].

Overall, our work provided a better understanding of the native structure of sNS1 in DENV pathogenesis. The functional role of HDL-bound NS1 protein in disease is now a topic of contention. Contrary to the known protective roles of HDL such as against endotoxic shock caused by lipopolysaccharides[47-51], Benfrid et al. (2022) showed that sNS1:HDL complex triggers proinflammatory signals when tested with primary human macrophages[20]. The presence of sNS1:HDL complexes as a predominant population of sNS1 in our *in vitro* infection model corroborates with a previous report of an interaction between insect-derived recombinant NS1 and the classical HDL/ApoA1-binding receptor known as SR-BI[17], which is expressed on hepatocytes[42]. This interaction in hepatocytes have been demonstrated to trigger endocytosis of sNS1 and subsequent downstream effects including vascular permeability, which is a

characteristic feature of severe dengue[17,52,53]. Internalisation of sNS1 is critical for increased virus production in hepatocytes[52] and NS1-mediated permeability in endothelial cells[53]. Furthermore, NS1:HDL complexes have been shown to induce the production of pro-inflammatory cytokines in macrophages and their presence has been detected in the sera of hospitalised DENV patients[20]. Yet, this hypothesis is confounded by other reports. While rsNS1 has been shown to trigger a TLR4-mediated release of proinflammatory cytokines to induce vascular leakage[54,55], Coelho et al. (2021) further showed that lipid-free recombinant ApoA1 neutralizes the proinflammatory effects caused by insect-derived recombinant intracellular NS1[55]. Furthermore, exogenous administration of purified HEK-293 derived NS1 failed to worsen *in vivo* vascular leakage in sublethally infected mice[43]. This underscores the need for physiologically relevant studies to reconcile these discrepancies and gain a comprehensive understanding of the role of NS1-HDL complex in DENV pathogenesis.

In conclusion, despite the study limitations that our isNS1wt and isNS1ts were immunoaffinity purified with one specific monoclonal antibody (Ab56.2), our structural model, obtained by CryoEM and verified by XL-MS, of infection-derived sNS1 shows a NS1 dimer embedded on a single HDL particle composed of ApoA1 dimer. Future investigation of this work using infected mouse sera from other DENV strains and different flaviviruses would inform the structural and functional relevance of the HDL-bound NS1 protein complex amongst flaviviral NS1 as well as provide a basis for the development of NS1-directed therapeutics.

References

1 Bhatt, S. *et al.* The global distribution and burden of dengue. *Nature* **496**, 504-507 (2013). https://doi.org:10.1038/nature12060

2 Diamond, M. S. & Pierson, T. C. Molecular Insight into Dengue Virus Pathogenesis and Its Implications for Disease Control. *Cell* **162**, 488-492 (2015). https://doi.org:10.1016/j.cell.2015.07.005

3 Libraty, D. H. *et al.* High circulating levels of the dengue virus nonstructural protein NS1 early in dengue illness correlate with the development of dengue hemorrhagic fever. *J Infect Dis* **186**, 1165-1168 (2002). https://doi.org:10.1086/343813

4 Paranavitane, S. A. *et al.* Dengue NS1 antigen as a marker of severe clinical disease. *BMC Infect Dis* **14**, 570 (2014). https://doi.org:10.1186/s12879-014-0570-8

5 Glasner, D. R., Puerta-Guardo, H., Beatty, P. R. & Harris, E. The Good, the Bad, and the Shocking: The Multiple Roles of Dengue Virus Nonstructural Protein 1 in Protection and Pathogenesis. *Annu Rev Virol* **5**, 227-253 (2018). https://doi.org:10.1146/annurev-virology-101416-041848

6 Watterson, D., Modhiran, N. & Young, P. R. The many faces of the flavivirus NS1 protein offer a multitude of options for inhibitor design. *Antiviral Res* **130**, 7-18 (2016). https://doi.org:10.1016/j.antiviral.2016.02.014

7 Scaturro, P., Cortese, M., Chatel-Chaix, L., Fischl, W. & Bartenschlager, R. Dengue Virus Non-structural Protein 1 Modulates Infectious Particle Production via Interaction with the Structural Proteins. *PLOS Pathogens* **11**, e1005277 (2015). https://doi.org:10.1371/journal.ppat.1005277

8 Plaszczyca, A. *et al.* A novel interaction between dengue virus nonstructural protein 1 and the NS4A-2K-4B precursor is required for viral RNA replication but not for formation of the membranous replication organelle. *PLoS Pathog* **15**, e1007736 (2019). https://doi.org:10.1371/journal.ppat.1007736

9 Puerta-Guardo, H., Glasner, D. R. & Harris, E. Dengue Virus NS1 Disrupts the Endothelial Glycocalyx, Leading to Hyperpermeability. *PLoS Pathog* **12**, e1005738 (2016). https://doi.org:10.1371/journal.ppat.1005738

10 Beatty, P. R. *et al.* Dengue virus NS1 triggers endothelial permeability and vascular leak that is prevented by NS1 vaccination. *Sci Transl Med* **7**, 304ra141 (2015). https://doi.org:10.1126/scitranslmed.aaa3787

11 Akey, D. L. *et al.* Flavivirus NS1 Structures Reveal Surfaces for Associations with Membranes and the Immune System. *Science* **343**, 881-885 (2014). https://doi.org:doi:10.1126/science.1247749

12 Xu, X. *et al.* Contribution of intertwined loop to membrane association revealed by Zika virus full-length NS1 structure. *EMBO J* **35**, 2170-2178 (2016). https://doi.org:10.15252/embj.201695290

13 Brown, W. C. *et al.* Extended surface for membrane association in Zika virus NS1 structure. *Nature Structural & Molecular Biology* **23**, 865-867 (2016). https://doi.org:10.1038/nsmb.3268

14 Flamand, M. *et al.* Dengue Virus Type 1 Nonstructural Glycoprotein NS1 Is Secreted from Mammalian Cells as a Soluble Hexamer in a Glycosylation-Dependent Fashion. *Journal of Virology* **73**, 6104-6110 (1999). https://doi.org:doi:10.1128/JVI.73.7.6104-6110.1999

15 Gutsche, I. *et al.* Secreted dengue virus nonstructural protein NS1 is an atypical barrel-shaped high-density lipoprotein. *Proc Natl Acad Sci U S A* **108**, 8003-8008 (2011). https://doi.org:10.1073/pnas.1017338108

16 Muller, D. A. *et al.* Structure of the dengue virus glycoprotein non-structural protein 1 by electron microscopy and single-particle analysis. *J Gen Virol* **93**, 771-779 (2012). https://doi.org:10.1099/vir.0.039321-0

17 Alcala, A. C. *et al.* Dengue Virus NS1 Uses Scavenger Receptor B1 as a Cell Receptor in Cultured Cells. *J Virol* **96**, e0166421 (2022). https://doi.org:10.1128/JVI.01664-21

18 Avirutnan, P. *et al.* Secreted NS1 of dengue virus attaches to the surface of cells via interactions with heparan sulfate and chondroitin sulfate E. *PLoS Pathog* **3**, e183 (2007). https://doi.org:10.1371/journal.ppat.0030183

19 Alcala, A. C. *et al.* The dengue virus non-structural protein 1 (NS1) is secreted from infected mosquito cells via a non-classical caveolin-1-dependent pathway. *J Gen Virol* **98**, 2088-2099 (2017). https://doi.org:10.1099/jgv.0.000881

20 Benfrid, S. *et al.* Dengue virus NS1 protein conveys pro-inflammatory signals by docking onto high-density lipoproteins. *EMBO Rep* **23**, e53600 (2022). https://doi.org:10.15252/embr.202153600

21 Rodriguez-Roche, R. *et al.* Virus evolution during a severe dengue epidemic in Cuba, 1997. *Virology* **334**, 154-159 (2005). https://doi.org:10.1016/j.virol.2005.01.037

22 Chan, K. W. K. *et al.* A T164S mutation in the dengue virus NS1 protein is associated with greater disease severity in mice. *Sci Transl Med* **11** (2019). https://doi.org:10.1126/scitranslmed.aat7726

23 Rozen-Gagnon, K., Moreland, N. J., Ruedl, C. & Vasudevan, S. G. Expression and immunoaffinity purification of recombinant dengue virus 2 NS1 protein as a cleavable SUMOstar fusion. *Protein Expr Purif* **82**, 20-25 (2012). https://doi.org:10.1016/j.pep.2011.11.003

24 Kitti, C. W. K. *THE ROLE OF GENETIC VARIANTS OF NON-STRUCTURAL PROTEIN 1 IN DENGUE PATHOGENESIS*, National University of Singapore, (2019).

25 Wu, S. *et al.* Fabs enable single particle cryoEM studies of small proteins. *Structure (London, England : 1993)* **20**, 582-592 (2012). https://doi.org:10.1016/j.str.2012.02.017

26 Bloch, J. S. *et al.* Structure and mechanism of the ER-based glucosyltransferase ALG6. *Nature* **579**, 443-447 (2020). https://doi.org:10.1038/s41586-020-2044-z

27 Jumper, J. *et al.* Highly accurate protein structure prediction with AlphaFold. *Nature* **596**, 583-589 (2021). https://doi.org:10.1038/s41586-021-03819-2

28 Mirdita, M. *et al.* ColabFold: making protein folding accessible to all. *Nature Methods* **19**, 679-682 (2022). https://doi.org:10.1038/s41592-022-01488-1

29 Biering, S. B. *et al.* Structural basis for antibody inhibition of flavivirus NS1-triggered endothelial dysfunction. *Science* **371**, 194-200 (2021). https://doi.org:10.1126/science.abc0476

30 Silva, R. A. *et al.* Structure of apolipoprotein A-I in spherical high density lipoproteins of different sizes. *Proc Natl Acad Sci U S A* **105**, 12176-12181 (2008). https://doi.org:10.1073/pnas.0803626105

31 He, Y. *et al.* Apolipoprotein A1 Forms 5/5 and 5/4 Antiparallel Dimers in Human High-density Lipoprotein. *Molecular & Cellular Proteomics* **18**, 854-864 (2019). https://doi.org:10.1074/mcp.RA118.000878

32 Kao, A. *et al.* Development of a Novel Cross-linking Strategy for Fast and Accurate Identification of Cross-linked Peptides of Protein Complexes. *Molecular & Cellular Proteomics* **10** (2011). https://doi.org:10.1074/mcp.M110.002212

33 Shu, B. *et al.* CryoEM structures of the multimeric secreted NS1, a major factor for dengue hemorrhagic fever. *Nature Communications* **13**, 6756 (2022). https://doi.org:10.1038/s41467-022-34415-1

34 Edeling, M. A., Diamond, M. S. & Fremont, D. H. Structural basis of Flavivirus NS1 assembly and antibody recognition. *Proc Natl Acad Sci U S A* **111**, 4285-4290 (2014). https://doi.org:10.1073/pnas.1322036111

35 Modhiran, N. *et al.* A broadly protective antibody that targets the flavivirus NS1 protein. *Science* **371**, 190-194 (2021). https://doi.org:10.1126/science.abb9425

36 Wang, D. *et al.* A Mutation Identified in Neonatal Microcephaly Destabilizes Zika Virus NS1 Assembly in Vitro. *Sci Rep* **7**, 42580 (2017). https://doi.org:10.1038/srep42580

37 Poonsiri, T. *et al.* Structural Study of the C-Terminal Domain of Nonstructural Protein 1 from Japanese Encephalitis Virus. *J Virol* **92** (2018). https://doi.org:10.1128/jvi.01868-17

38 Low, J. G. *et al.* Efficacy and safety of celgosivir in patients with dengue fever (CELADEN): a phase 1b, randomised, double-blind, placebo-controlled, proof-of-concept trial. *The Lancet Infectious Diseases* **14**, 706-715 (2014). https://doi.org:10.1016/s1473-3099(14)70730-3

39 Malajczuk, C. J., Gandhi, N. S. & Mancera, R. L. Structure and intermolecular interactions in spheroidal high-density lipoprotein subpopulations. *J Struct Biol X* **5**, 100042 (2021). https://doi.org:10.1016/j.yjsbx.2020.100042

40 Young, P. R., Hilditch, P. A., Bletchly, C. & Halloran, W. An antigen capture enzyme-linked immunosorbent assay reveals high levels of the dengue virus protein NS1 in the sera of infected patients. *J Clin Microbiol* **38**, 1053-1057 (2000). https://doi.org:10.1128/JCM.38.3.1053-1057.2000

41 Alcon, S. *et al.* Enzyme-linked immunosorbent assay specific to Dengue virus type 1 nonstructural protein NS1 reveals circulation of the antigen in the blood during the acute phase of disease in patients experiencing primary or secondary infections. *J Clin Microbiol* **40**, 376-381 (2002). https://doi.org:10.1128/JCM.40.02.376-381.2002

42 Kontush, A. *et al.* Structure of HDL: particle subclasses and molecular components. *Handb Exp Pharmacol* **224**, 3-51 (2015). https://doi.org:10.1007/978-3-319-09665-0_1

43 Gordon, S. M. & Remaley, A. T. High density lipoproteins are modulators of protease activity: Implications in inflammation, complement activation, and atherothrombosis. *Atherosclerosis* **259**, 104-113 (2017). https://doi.org:10.1016/j.atherosclerosis.2016.11.015

44 Puerta-Guardo, H. *et al.* Flavivirus NS1 Triggers Tissue-Specific Vascular Endothelial Dysfunction Reflecting Disease Tropism. *Cell Rep* **26**, 1598-1613.e1598 (2019). https://doi.org:10.1016/j.celrep.2019.01.036

45 Ooi, J. S. G. & Lok, S. M. How NS1 Antibodies Prevent Severe Flavivirus Disease. *Trends Biochem Sci* **46**, 519-521 (2021). https://doi.org:10.1016/j.tibs.2021.03.005

46 van den Elsen, K., Chew, B. L. A., Ho, J. S. & Luo, D. Flavivirus nonstructural proteins and replication complexes as antiviral drug targets. *Current Opinion in Virology* **59**, 101305 (2023). https://doi.org:https://doi.org/10.1016/j.coviro.2023.101305

47 Levine, D. M., Parker, T. S., Donnelly, T. M., Walsh, A. & Rubin, A. L. In vivo protection against endotoxin by plasma high density lipoprotein. *Proc Natl Acad Sci U S A* **90**, 12040-12044 (1993). https://doi.org:10.1073/pnas.90.24.12040

48 Wurfel, M. M., Kunitake, S. T., Lichenstein, H., Kane, J. P. & Wright, S. D. Lipopolysaccharide (LPS)-binding protein is carried on lipoproteins and acts as a cofactor in the neutralization of LPS. *J Exp Med* **180**, 1025-1035 (1994). https://doi.org:10.1084/jem.180.3.1025

49 Trinder, M., Walley, K. R., Boyd, J. H. & Brunham, L. R. Causal Inference for Genetically Determined Levels of High-Density Lipoprotein Cholesterol and Risk of Infectious Disease. *Arteriosclerosis, Thrombosis, and Vascular Biology* **40**, 267-278 (2020). https://doi.org:doi:10.1161/ATVBAHA.119.313381

50 Tall, A. R. HDL in Morbidity and Mortality: A 40+ Year Perspective. *Clinical Chemistry* **67**, 19-23 (2020). https://doi.org:10.1093/clinchem/hvaa148

51 Harslof, M., Pedersen, K. M., Afzal, S., Davey Smith, G. & Nordestgaard, B. G. Lower levels of small HDL particles associated with increased infectious disease morbidity and mortality: a population-based cohort study of 30 195 individuals. *Cardiovasc Res* **119**, 957-968 (2023). https://doi.org:10.1093/cvr/cvac194

52 Alcon-LePoder, S. *et al.* The secreted form of dengue virus nonstructural protein NS1 is endocytosed by hepatocytes and accumulates in late endosomes: implications for viral infectivity. *J Virol* **79**, 11403-11411 (2005). https://doi.org:10.1128/JVI.79.17.11403-11411.2005

53 Wang, C. *et al.* Endocytosis of flavivirus NS1 is required for NS1-mediated endothelial hyperpermeability and is abolished by a single N-glycosylation site mutation. *PLoS Pathog* **15**, e1007938 (2019). https://doi.org:10.1371/journal.ppat.1007938

54 Modhiran, N. *et al.* Dengue virus NS1 protein activates cells via Toll-like receptor 4 and disrupts endothelial cell monolayer integrity. *Sci Transl Med* **7**, 304ra142 (2015). https://doi.org:10.1126/scitranslmed.aaa3863

55 Coelho, D. R. & Carneiro, P. H. Expression and Purification of Dengue NS1 Protein in Sf9-Baculovirus System. *Methods Mol Biol* **2409**, 39-46 (2022). https://doi.org:10.1007/978-1-0716-1879-0_4

56 Perez-Riverol, Y. *et al.* The PRIDE database resources in 2022: a hub for mass spectrometry-based proteomics evidences. *Nucleic Acids Research* **50**, D543-D552 (2021). https://doi.org:10.1093/nar/gkab1038

Acknowledgments

We thank the scientific facility support from NTU Institute of Structural Biology and Protein Product Platform. The authors acknowledge the Cryo-Electron Microscopy Facility at Center for Bioimaging Science, Department of Biological Science, National University of Singapore the scientific and technical assistance. Recombinant DENV2 NS1 protein is a generous gift from Dr Shu Bo and Professor Lok Shee Mei. We thank members of the DL and SV labs for their support.

Funding: This research is supported by the Singapore Ministry of Education under its Singapore Ministry of Education Academic Research Fund Tier 2 (T2EP30220-0020) to DL and National Medical Research Council of Singapore (MOH-OFIRG18may-0006; MOH-OFIRG20nov-0002) to SV, A*STAR core funding and Singapore National Research Foundation under its NRF-SIS "SingMass" scheme to R.M.S, Career Development Award 2021 (A*STAR BMRC) to W.W.P., Career Development Fund 2021 (A*STAR BMRC) to S.Z., and LKCMedicine Dean's Postdoctoral Fellowship to C.B.L.A.

Author contributions: Conceptualization: SV and DL; Investigation: BLAC, AQN, WWP, KWKC, ZS, SSL, MJGW, MMC, JGL, EEO, SV and DL; Writing: BLAC, AQN, SV, and DL with input from all authors.

Competing interests: Authors declare that they have no competing interests.

Data availability:

The data that support this study are available from the corresponding authors upon reasonable request. The cryoEM density maps have been deposited in the Electron Microscopy Data Bank (EMDB) under accession codes EMD-36483 (isNS1ts:Fab56.2) and EMD-36480 (Fab56.2:isNS1ts:HDL). The crosslinking MS raw files and the search results can be downloaded from **https://repository.jpostdb.org/preview/14869768463bf85b347ac2** with the access code: 3827. The HDX-MS data is deposited to the ProteomeXchange consortium via PRIDE partner repository[56] with the dataset identifier PXD042235.